

# The Reduced Paleostress Tensors Based on Fault-Slip Data of Dana Conglomerate Formation in Ed Dhira Area, Dead Sea-Jordan

Mohammad Al-Adamat\* and Abdullah Diabat

Department of Applied Earth and Environmental Sciences, Faculty of Earth and Environmental Sciences, Al al-Bayt University, Al-Mafraq-Jordan

Received 15<sup>th</sup> February 2022; Accepted 29<sup>th</sup> April 2022

## Abstract

This study presents paleo stress results based on fault-slip data measured in the Dana Conglomerate Formation (Neogene) in Ed Dhira area east of the Dead Sea basin. Stress inversion of fault-slip data was carried out utilizing an improved Right-Dihedral method, followed by rotational optimization. Results revealed the existence of a strike-slip regime in all stress tensors, in which  $\sigma_1$  (SHmax) and  $\sigma_3$  (Shmin) are usually sub-horizontal and  $\sigma_2$  is sub-vertical. The stress ratio (R) ranged between 0.25 - 0.67 and the stress index (R') ranged between 1.33- 1.75. The SHmax  $\sigma_1$  oriented ESE– WNW within a range of 15° (113- 128) of all stress tensors. The results revealed about 10°-20° anti-clockwise rotation compared with the main trend of the Dead Sea stress (NW-SE SHmax) to WNW-ESE trend in the study area. The stress variations are due to the block rotation along the main faults in the study area and/ or may be due to stress changes in time.

© 2022 Jordan Journal of Earth and Environmental Sciences. All rights reserved

**Keywords:** Paleostress, Dana Conglomerate, Neogene, Dead Sea Transform, Jordan.

## 1. Introduction

Paleostress analysis aims to classify stress systems acting in the past from their record in deformation structures, singularly from fault-slip data (Simón, 2019). Determination of the paleo stress tensors is an essential tool to characterize successive tectonic episodes in deformed rock (Radaideh and Melichar, 2015). The direction of the paleo stress can be determined successfully depending on the analysis of different types of geological structures, such as faults, fold axes, joints, veins, stylolites, and dykes (Zoback, 1992). Collections of small faults from a restricted area like an outcrop or a quarry can be analyzed to reconstruct the local paleo stress field (Fossen, 2016). Meso-scale faults are common. Their data can be widely collected, and their mechanical analysis provides the reconstruction of the successive stress states (Hardy et al., 2010). They are more widely used than large-scale faults to determine the stress field with a greater spatial resolution (Yamaji, 2007). Determinations of reduced stress tensors using fault slip data yield the orientation of principal stress axes and the ratio  $\Phi$  or R of the differences between principal stress magnitudes. The use of rupture and friction laws allows the determination of the two remaining unknowns, that is, the reconstruction of the complete stress tensor (Angelier, 1989).

The goal of paleo stress inversion is to characterize what is known as the reduced stress tensor (Igwe and Okonkwo, 2016.) The reduced stress tensor has four parameters to define the full stress tensor: the principal stress axes  $\sigma_1$  (maximum compression),  $\sigma_2$  (intermediate compression), and  $\sigma_3$  (minimum compression), and the Stress Ratio  $R = (\sigma_2 - \sigma_3) / (\sigma_1 - \sigma_3)$  (Delvaux and Sperner, 2003). Moreover, multiple methods for paleo stress analysis have been developed from the concept of stress inversion

(e.g., Žalohar and Verbac, 2007; Delvaux and Sperner, 2003; Yamaji, 2000; Sperner, et al.,1993; Angelier and Mechler, 1977). The application of these methods is based on Wallace and Bott hypothesis (Bott, 1959; Wallace, 1951), which describes that the direction of slip in planar structure is parallel to the maximum shear stress of the reduced stress tensor.

The area being studied is located within the Ed Dhira area, to the east of the Dead Sea Basin (DSB). The DSB is a part of the most magnificent structural element in the region, the Dead Sea Transform Fault (DSTF) (Figures 1a and b). Furthermore, the Dana Conglomerates Formation (DC) is a clastic deposit that was formed during a significant episode of uplift and erosion following the regression of the Tethys Ocean in the late Eocene (Khalil, 1992). It is deposited in tectonically unstable basins during an extensional tectonic stage related to an early rifting phase (Powell, 1988). This research aims to shed light on the paleostresses of the DC Formation in five established measurement stations based on fault-slip data, as no research has been conducted in the current study area.

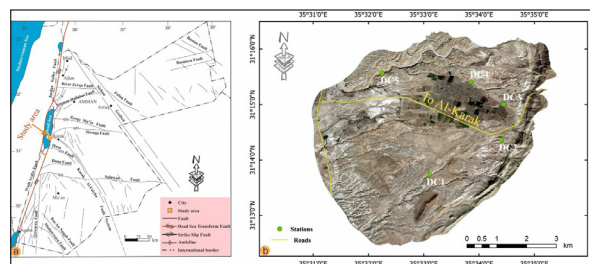


**Figure 1.** Structural setting of the study area. (a) The structural pattern of Jordan shows the location of the study area (modified from Diabat and Masri, 2005), and (b) a Satellite image of the study area with the established field measurement stations.

\* Corresponding author e-mail: m.aladamat90@gmail.com

## 2. Geological setting

### 2.1. Stratigraphy

The outcropping rocks in the area under investigation range from the Upper Cretaceous to the Quaternary (Figure 2 a and b).

Era	Period	Epoch	Group	Formation	General lithology
Cenozoic	Quaternary	Recent-Holocene		Surficial Deposits	Soil, sand and gravel
		Pleistocene		Lisan	Marl, gypsum and clay
	Tertiary	Pliocene		Dana Conglomerate	Mixed clastics in cycles: conglomerate and calcarenite
		Miocene			
		Oligocene			
		Eocene		Umm Rijam	Chert and limestone
Cenozoic	Cretaceous	Upper	Maastrichtian	Muwaqqar	Chalk
			Campanian	Amman	Chert interbedded with silicified limestone
			Santonian	Wadi Umm Ghudran	Chalk
			Coniacian	Wadi As Sir	Massive Limestone
		Lower	Turonian	Fuhis Hummar-Shaib (undifferentiated)	Marl, limestone and marly limestone
				Naur	Limestone

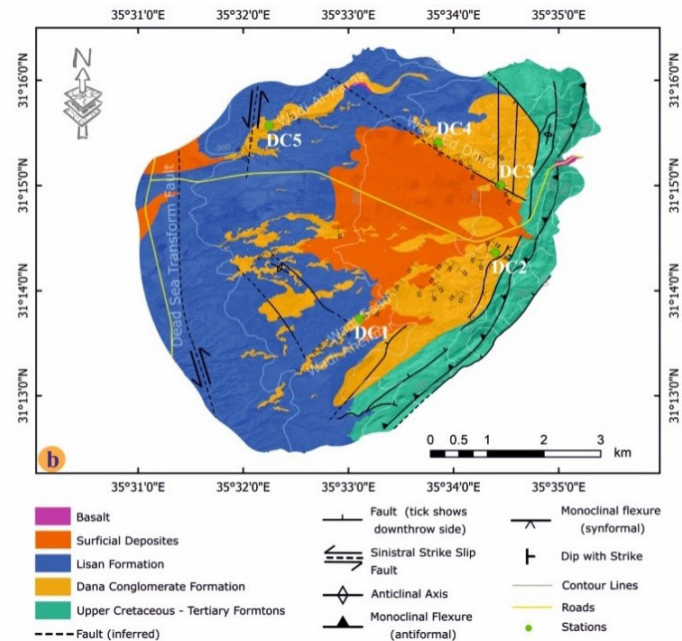


**Figure 2.** (a) The lithostratigraphic units exposed in the study area (modified from Powel 1988; Khalil 1992), and (b) the Geological map of the study area with the established field measurement stations.

#### 2.1.1. Dana Conglomerate Formation (Oligo-Pliocene)

The formation is exposed in different locations within the study area (Figure 2b). According to Powell (1988), this formation can be divided into informal lower- and upper-members which are equivalent to the subdivision of Bender (1974), who also pointed to this unit as the Syn-tectonic Conglomerate. Moreover, the lower member is composed of thick beds of pebble-boulder conglomerate comprising poorly graded, well-rounded, clast of chert, chalk, and chalky limestone which derived from the Eocene formations (Powell, 1988 and Khalil, 1992). The formation's upper member is made up of thick beds of clast-supported, poorly sorted, a well-rounded pebble-to-boulder conglomerate with a calcarenite/siliciclastic matrix. The lower member has a distinctive pink-tan and white color in the field, while the top member weathers to a brown-yellow tone (Powell, 1988). As it was mentioned earlier the formation has deposited in tectonically unstable basins during an extensional tectonic phase related to an early rifting stage.

#### 2.2. Tectonic Setting

The Dead Sea Transform Fault (DSTF) is a left-lateral strike-slip fault system, about 1100 km in length (Masson et al., 2015). It accommodates strike-slip motion between the Sinai sub-plate to the West and the Arabian plate to the East (Weinstein et al., 2020). It links the Red Sea spreading center in the south to the Bitlis-Zagros zone of plate convergence in southern Turkey to the north (Figure 3a) (Khon et al., 2019). The DSTF is composed of numerous fault segments and associated transtensional and transpressional features, such as pull-apart basins, fault escarpments, and pressure ridges (Atallah and Al-Taj 2004; Atallah 1992; Garfunkel 1981). In Jordan, the DSTF comprises two main segments, the Wadi Araba Fault (WAF) in the south and the Jordan Valley Fault (JVF) in the north, which bound the Dead Sea Basin (DSB) in the middle (Figure 3b) (Garfunkel 1981). The DSB is an elongated deep Pull-apart basin, whose overall

length is about 150 km, and its width ranges between 15–20 km (Wetzler, et al., 2015). Nevertheless, in the study area, the main DSTF is not exposed at the surface, but its trace is inferred depending on the geomorphology and geophysical pieces of evidence (Powell, 1988 and Khalil, 1992)

Ed Dhira area lies on the eastern flank of the DSB. It is surrounded by the Ed Dhira Monocline and splay fault to the east, and the Siwaqa fault to the northeast (Figure 3c) (Masri, 1997). The majority of the folds formed in the area are related to flexural juxtaposes of the associated faults; these include the Ed Dhira fault-monocline which is the main flexure spanning from the Siwaqa fault in the north to Wadi Assal in the south. It forms an arc-like structure trending NNW in the north, N in the middle, and NE in the southern part (Powell, 1988) (Figure 3c). Ed Dhira fault is a significant NE-SW trending splay fault that branches off the main DSTF in the vicinity of Wadi Assal, about 3.5 kilometers south of the studied area. The beds along the fault trace are frequently crushed or shattered by small faults. This fault disappears and passes into a main monoclinial flexure with minor faults (Powell, 1988) (Figure 3c). Rhomb-shaped faulted blocks are bounded by N-S and NW-SE trending faults and are well preserved in strata of the DC Formation in the Ed Dhira area (Figure 2b) (Khalil, 1992). A study carried out by Al-Adamat and Diabat (2021) in Ed Dhira area, proved the occurrence of syn-depositional extensional structures as normal faults and associated systems like horsts and grabens, joints, plumose joints, tension gashes, and veins. Horst and graben structures with a displacement range from a few centimeters to more than 3 m were observed in three stations of the study area, indicating N-S, NE-SW, and E-W extensional directions, respectively. In addition to negative flowers, the structure was observed in two stations associated with N-S- and NW-SE-directed strike-slip faults. This is explained as transmission related to the Dead Sea stress field.

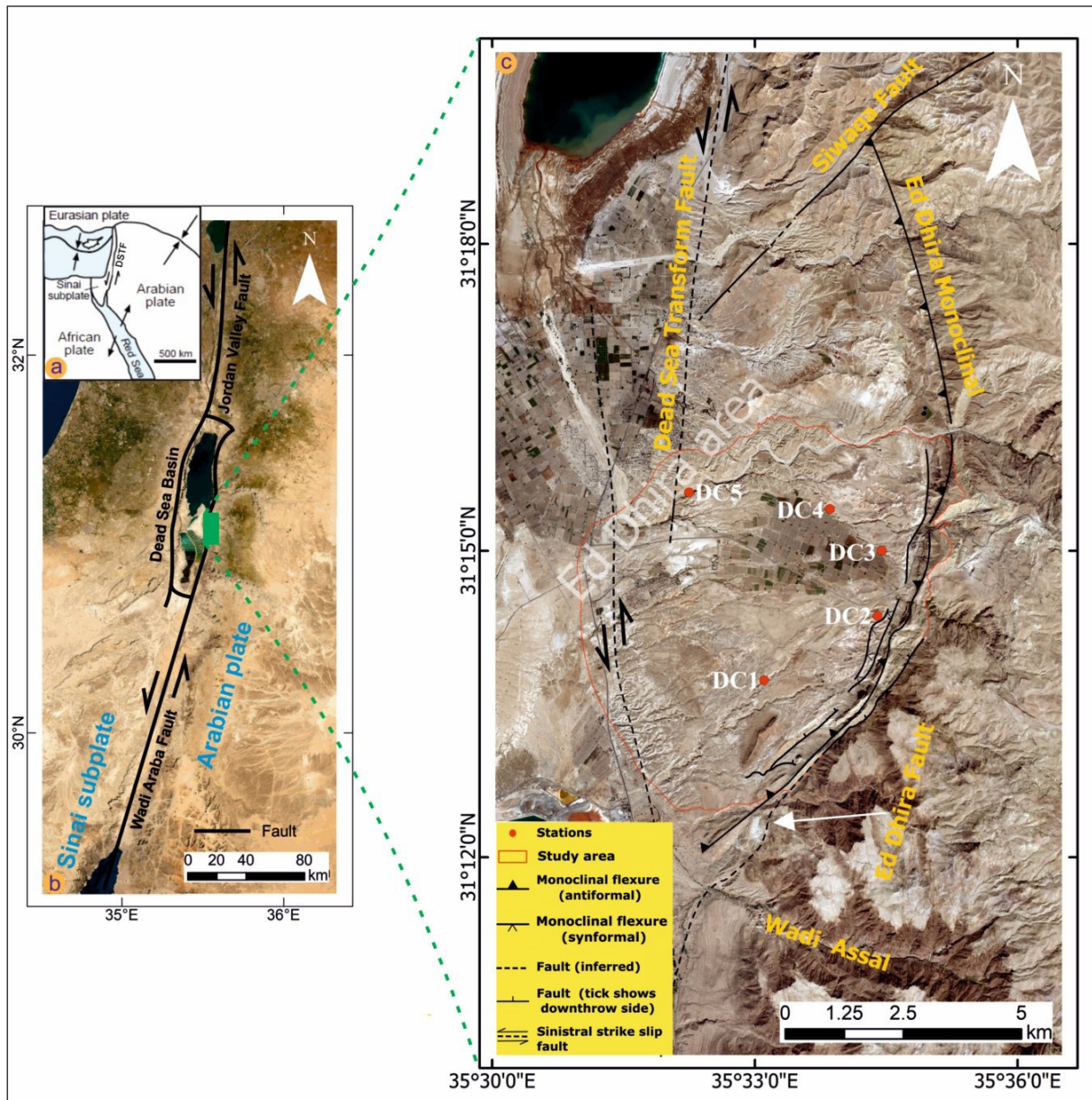


**Figure 3.** (a) Tectonic setting of the DSTF, (b) Satellite image of the DSTF segments in Jordan, and (c) Satellite image showing the tectonic setting of Ed Dhira area and the main geological structures of the study area.

**3. Methodology**

The study was dependent mainly on the fieldwork which has been included five investigated measurement stations. Collecting data have been performed by measuring the dip and strike of faults, and the trend and plunge of slickenlines on the fault planes within the Dana Conglomerate Formation. Field data including fault planes with slip lines and sense of movement have been used to calculate the orientation of the principal stresses ( $\sigma_1$ ,  $\sigma_2$ , and  $\sigma_3$ ): the principal stress axis  $\sigma_1$  (maximum compression),  $\sigma_2$  (intermediate compression) and  $\sigma_3$  (minimum compression) and the ratio of principal stress difference  $R = (\sigma_2 - \sigma_3) / (\sigma_1 - \sigma_3)$  which characterize the shape of the stress tensor, have been determined using successively the improved right dihedron method (Angelier and Mechler, 1977) and the rotational optimization method (Delvaux and Sperner, 2003). Both methods have been applied to utilize a free source computer software named Win Tensor (Delvaux, 2012). It is widely used by several geologists for reconstruction fractures analysis and crustal

stresses. Moreover, the stress tensors are divided into the following: radial /pure/ strike-slip extensive, extensive / pure/ compressive strike-slip, or strike-slip, pure, radial compressive depending on the relative magnitude of the intermediate axis and given by stress ratio R (Delvaux et al.,1997) (Figure 4). On the geological map of the studied area, these tensors are exhibited with the orientation of both horizontal principal stress (SHmax) and horizontal minimum stress axes (Shmin).

Stress Tensor Type	EXTENSIVE			STRIKE-SLIP			COMPRESSIVE			
Stress Symbols										
Stress Ratio R	1.00	0.75	0.50	0.50	0.25	0.00	0.25	0.50	0.75	1.00
Stress Regime	Radial EXTENSIVE	Pure EXTENSIVE	TRANSVERSE	Pure STRIKE-SLIP	TRANSVERSE	Pure COMPRESSIVE	Radial COMPRESSIVE	COMPRESSIVE	COMPRESSIVE	Radial COMPRESSIVE
Stress Index R	R = R			R = 2-R			R = 2+R			

**Figure 4.** Stress tensor representation for different stress regimes (after Delvaux et al.,1997).

#### 4. Results

Based on the availability and accessible data, the studied area has been divided into five stations (Figure 3c). The fault-

slip data measurements have been performed by measuring slickenside lineations on the fault planes (Figure 5).

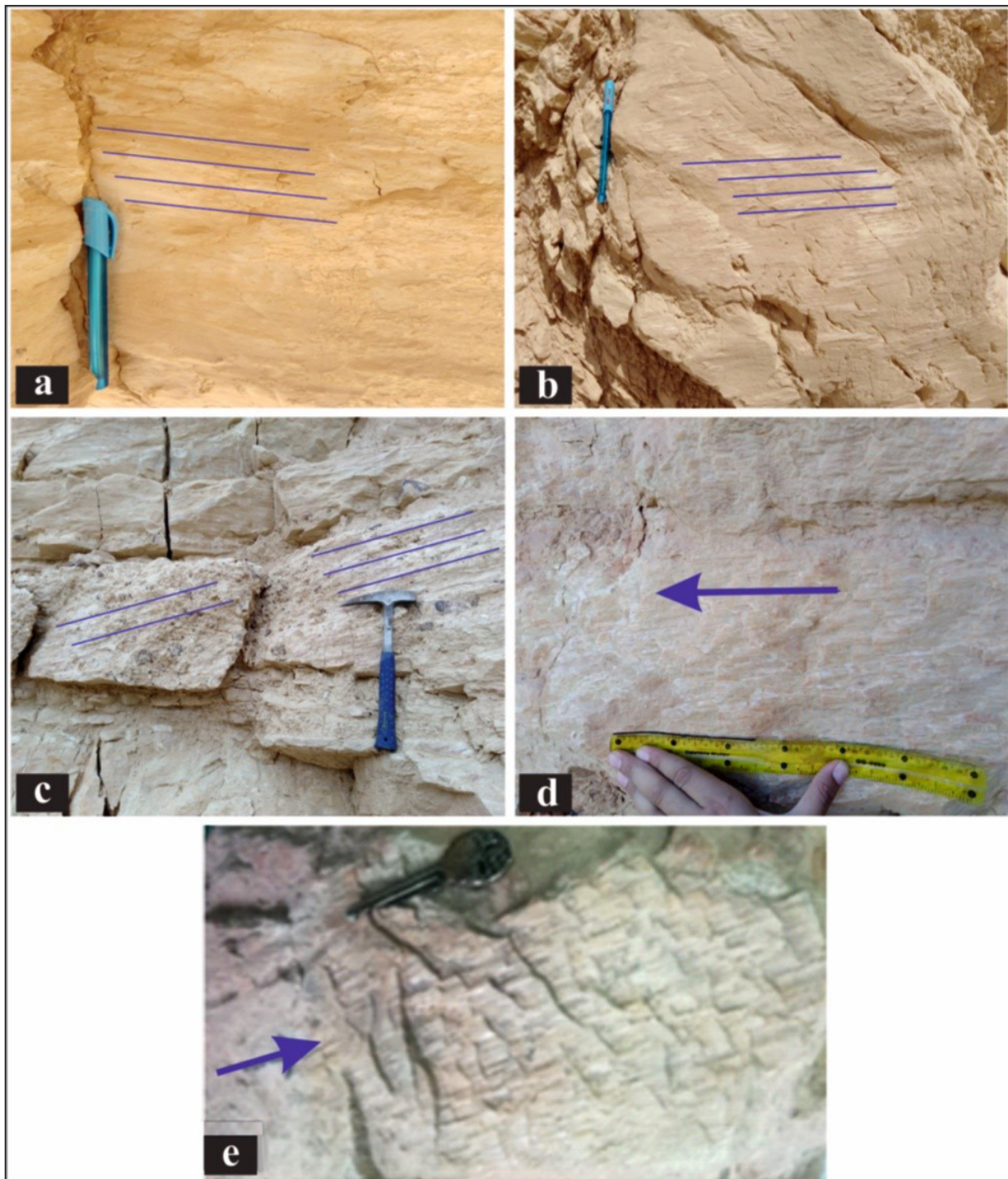


**Figure 5.** Kinematic indicators along the fault planes in the study area; (a and b) Horizontal slickenside lineations, (c) Oblique slickenside lineations, and (d & e) Mineral steps of dextral and sinistral movement, respectively.

##### 4.1. Field station DC1

This station is situated at Wadi Saad (as it is known locally) (Figure 2b). In this station, ten fault-slip data measurements were performed. After applying the improved right dihedral and rotational optimization methods respectively, the consequences show that the stress tensor is

characterized by  $\sigma_1$ : 25/293,  $\sigma_2$ : 65/100, and  $\sigma_3$ : 05/ 201 with  $R = 0.25$ . It belongs to a pure strike-slip regime and indicates WNW–ESE compression NNE –SSW extension (Figures 6a and b). This stress tensor produced the N–S to NNW–SSE sinistral strike-slip faults in the studied area.

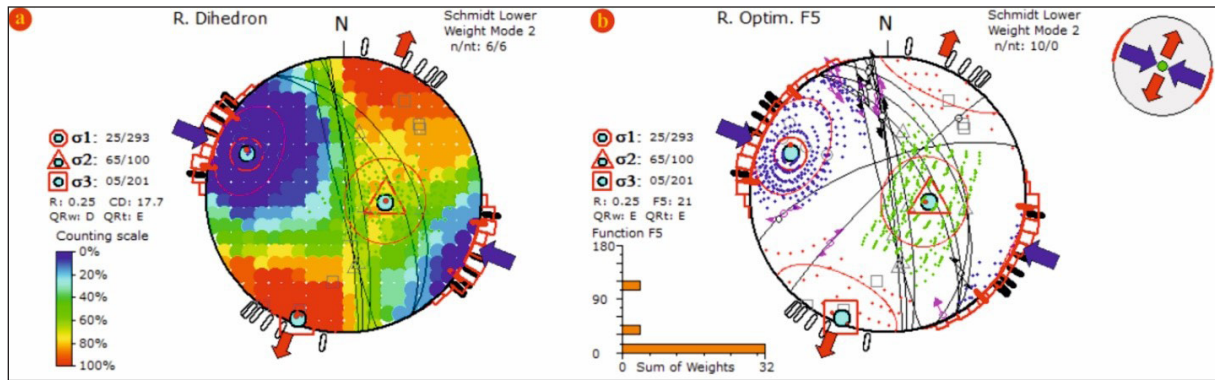


**Figure 6.** (a and b). Stress tensor shows WNW–ESE compression and NNE–SSW extension; Inward arrows represent compression, outward arrows denote tension, the circle is  $\sigma_1$ , the triangle indicates  $\sigma_2$  and the square is  $\sigma_3$  orientation.

**4.2. Field station DC2**

The station lies about 220 m from Al-Karak- Dead Sea Road (Figure 2b). Nine fault-slip data measurements were performed in DC2. After applying the improved right dihedron and rotational optimization methods separately, the outcomes show that the stress tensor is characterized by  $\sigma_1$ :

04/293,  $\sigma_2$ : 80/179, and  $\sigma_3$ : 09/ 024 with  $R = 0.56$ . It belongs to the pure strike-slip regime and indicates NNE–SSE extension and WNW– ESE compression (Figures 7a and b). This stress tensor is accountable for the formation of NNW–SSE sinistral strike-slip faults in the studied area.

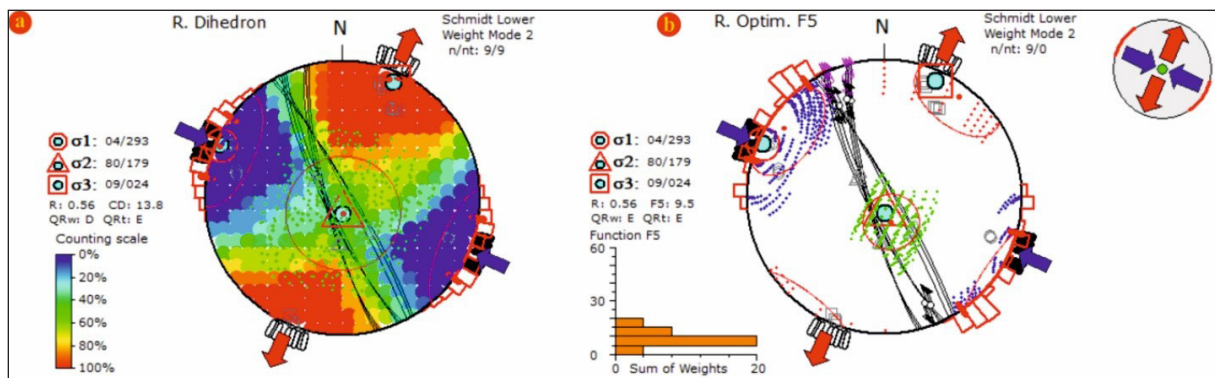


**Figure 7.** (a and b). Stress tensor shows NNE–SSE extension and WNW– ESE compression; Inward arrows denote compression, outward arrows represent tension, the circle is  $\sigma_1$ , the triangle is  $\sigma_2$  and the square indicates  $\sigma_3$  orientation.

**4.3. Field station DC3**

This station is located at Wadi Wadeaa (as it is known locally) (Figure 2b). Here, twenty-five fault-slip data measurements were carried out in the analysis. After applying the improved right dihedron and rotational optimization methods, the result is the stress tensor which is characterized

by  $\sigma_1$ : 11/300,  $\sigma_2$ : 67/182, and  $\sigma_3$ : 20/ 034 with  $R = 0.54$ . It belongs to the pure strike-slip regime and indicates NNE–SSE extension and WNW – ESE compression (Figures 8a and b). This stress tensor is responsible for the formation of conjugated NNW–SSE sinistral strike-slip faults and ENE–WSW dextral strike-slip faults in the studied area.

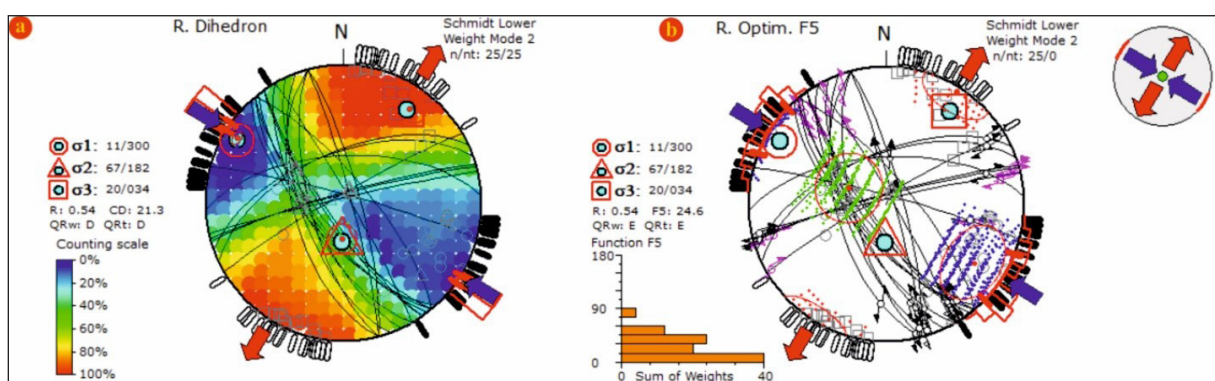


**Figure 8.** (a and b). Stress tensor shows NNE – SSE extension and WNW – ESE compression; Inward arrows represent compression, outward arrows denote tension, the circle is  $\sigma_1$ , the triangle indicates  $\sigma_2$  and the square is  $\sigma_3$  orientation.

4.4. Field station DC4

The DC4 is situated at Wadi Ed-Dhira (Figure 2b). Nine fault-slip data measurements were performed at this location. After applying the improved right dihedron and rotational optimization methods separately, the outcomes show that

the stress tensor is characterized by  $\sigma_1$ : 23/308,  $\sigma_2$ : 62/162, and  $\sigma_3$ : 14/ 044 with  $R = 0.67$ . It belongs to the pure strike-slip regime and indicates NE–SE extension and NW – SE compression (Figures 9a and b). This stress tensor produced the N–S sinistral strike-slip faults in the studied area.

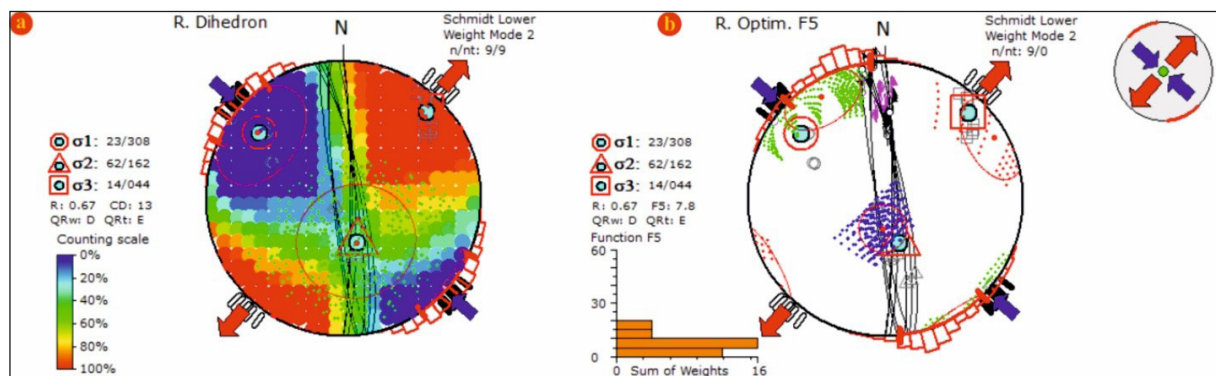


Figure 9. (a and b). Stress tensor shows extension and NW–SE compression; Inward arrows denote compression, outward arrows represent tension, the circle is  $\sigma_1$ , the triangle is  $\sigma_2$  and the square indicates  $\sigma_3$  orientation.

4.5. Field station DC5

The station lies at Wadi Al-Karak, northwestern of the study area (Figure 2b). Twenty-two fault-slip data measurements were carried out. After applying the improved right dihedron and rotational optimization methods respectively, the results show that the stress tensor

is characterized by  $\sigma_1$ : 02/123,  $\sigma_2$ : 85/236, and  $\sigma_3$ : 04/ 033 with  $R = 0.45$ . It belongs to the pure strike-slip regime and indicates NNE–SSE extension and WNW – ESE compression (Figures 10a and b). This stress tensor is responsible for the development of conjugated NNW–SSE sinistral strike-slip faults and E–W to ENE–WSW in the studied area.

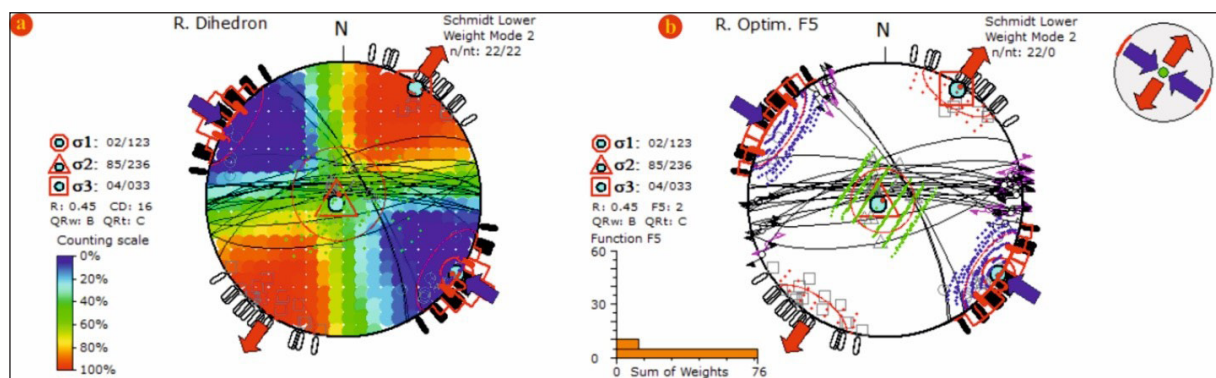


Figure 10. (a and b). The stress tensor shows NNE–SSE extension and WNW– ESE compression. Inward arrows represent compression, outward arrows denote tension, the circle is  $\sigma_1$ , the triangle indicates  $\sigma_2$  and the square is  $\sigma_3$  orientation.

5. Discussion

From the data in Table 1 and Fig. 11, it is noticed that all of the stress tensors belong to the pure strike-slip regime as R ratios range between 0.25 – 0.67, and the stress index ( $R'$ ) ranges between 1.33 – 1.75. The calculated results of stress inversion indicate that  $\sigma_1$  (SHmax) and  $\sigma_3$  (SHmin) are generally sub-horizontal and  $\sigma_2$  is sub-vertical in all the

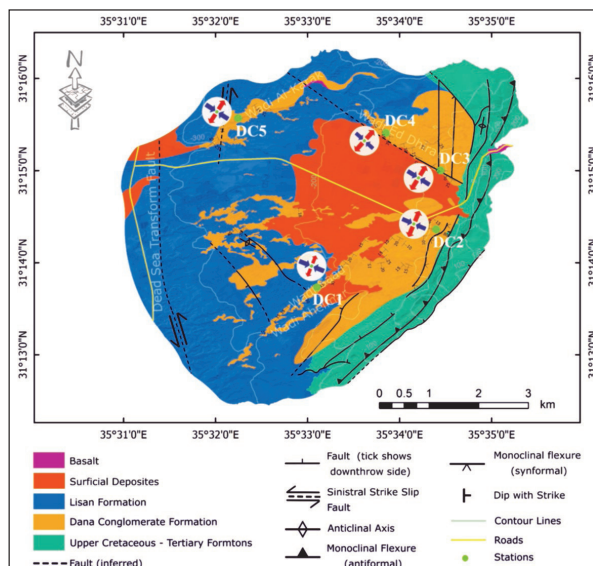
previous stress tensors, which are belonging to the strike-slip system with  $\sigma_1$  swinging around NW-SE to WNW- ESE direction within a range of 15 degrees (113- 128). These stress tensors are mainly responsible for the conjugated NW sinistral with E–W dextral, N–S to NNW sinistral with ENE to E–W dextral strike-slip faults in the study area at the later stage of deformation (Figs 6-10).

Table 1. Shows the results of the reduced paleo stress tensors obtained from the fault-slip data.

Station. No	N	R	R'	Principal Stress axis			Tensor type	SHmax
				$\sigma_1$	$\sigma_2$	$\sigma_3$		
1	10	0.25	1.75	25/293	65/100	05/201	Pure strike-slip	113
2	9	0.56	1.44	04/293	80/179	09/024	Pure strike-slip	113
3	25	0.54	1.46	11/300	67/182	20/034	Pure strike-slip	120
4	9	0.67	1.33	23/308	62/162	14/044	Pure strike-slip	128
5	22	0.45	1.55	02/123	85/236	04/033	Pure strike-slip	123

N= net data number representing the tensor.  
 $R = (\sigma_2 - \sigma_3) / (\sigma_1 - \sigma_3)$ .  
 $R'$  = tensor type index.

$\sigma_1, \sigma_2, \sigma_3$  = plunge, and azimuth of principal stress axes.  
 SHmax= maximum horizontal compressive stress.



**Figure 11.** Results of the stress inversion are represented as SHmax (blue arrows) and SHmin (red arrows) in the study area displayed on the geological map.

The stress tensors of the study area revealed an anti-clockwise rotation of 10-20 degrees for  $\sigma_1$  (SHmax) compared with the Dead Sea stress field (Figure. 12).

Stress inversion results in the study area also reveal slight differences in the direction of the principal stresses between some stations. This reflects the stress changes due to the position along the main faults and to block rotation, or they may also be due to stress changes in time. So, the stress state at any point along the main faults is the superposition of the regional tectonic stresses, which are generally uniform over relatively large areas (compared to the length of the faults) for a distinct tectonic event and a distinct stress field. The local fault-related stresses are affected by the displacement along the main faults and depend upon the position around them (Diabat, 2007).

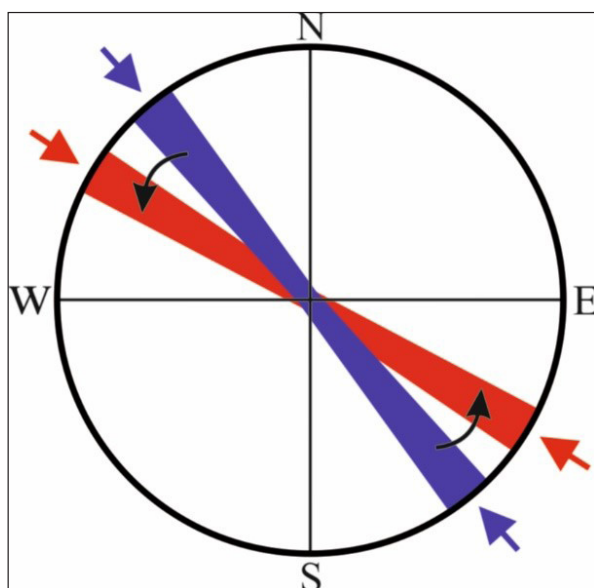


**Figure 12.** Directional model showing an anti-clockwise rotation of the maximum horizontal compression (SHmax); Dead Sea stress (blue), study area stress (red).

## 6. Conclusions

The current research has pointed out and elaborated on the state of paleo stress in the Ed Dhira area east of the Dead Sea. The results have shown that  $\sigma_1$  (SHmax) and  $\sigma_3$  (Shmin) are usually sub-horizontal and  $\sigma_2$  is sub-vertical in all stations, which are belonging to a major strike-slip system with  $\sigma_1$  SHmax swinging around the NW-SE to WNW-ESE direction. This revealed an anti-clockwise rotation of 10°-20° for  $\sigma_1$  (SHmax) compared with the Dead Sea stress field. The stress tensors are responsible for the formation of N-S to NNW-SSE sinistral strike-slip faults (e.g., DC1, DC2, and DC4), as well as the formation of conjugated NNW-SSE sinistral strike-slip faults with dextral E-W to ENE-WSW (e.g., DC3, and DC5) in the studied area.

## References

- Al-Adamat, M. and Diabat, A. (2021). Syndepositional extensional structures in Oligo-Pliocene Dana Conglomerate Formation at Ed Dhira area (Dead Sea, Jordan). *Arabian Journal of Geosciences*, 14: 309. <https://doi.org/10.1007/s12517-021-06666-7>.
- Angelier, J. (1989). From orientation to magnitudes in paleostress determinations using fault slip data. *Journal of Structural Geology*, 11 (1-2): 37-50. [https://doi.org/10.1016/0191-8141\(89\)90034-5](https://doi.org/10.1016/0191-8141(89)90034-5).
- Atallah, M. (1992). Tectonic evolution of northern Wadi Araba, Jordan. *Tectonophysics*, 204(1-2): 17-26. [https://doi.org/10.1016/0040-1951\(92\)90266-9](https://doi.org/10.1016/0040-1951(92)90266-9).
- Atallah, M., and Al-Taj, M. (2004). Active surface ruptures of the Dead Sea Transform in Wadi Araba, Jordan. *Dirasat, series B: Pure Sciences*, 31(1): 59-81.
- Bender, F. (1974). *Geology of Jordan*. Bontrager, Berlin.
- Bott, M. H. P. (1959). The Mechanics of Oblique Slip Faulting. *Geological Magazine*, 96(2): 109-117. <https://doi.org/10.1017/S0016756800059987>.
- Delvaux, D. (2012). Release of program Win-Tensor 4.0 for tectonic stress inversion: statistical expression of stress parameters. In: *Geophysical research abstracts*, 14. EGU General Assembly Vienna.
- Delvaux, D. and Sperner, B. (2003). New aspects of tectonic stress inversion with reference to the TENSOR program. In: Nieuwland, D. A. (Ed). *New Insights into Structural Interpretation and Modelling*. Special Publications, Geological Society, London. Pp.75-100.
- Delvaux, D., Moeys, R., Stapel, G., Petit, C., Levi, K., Miroshnichenko, A., and San'kov, V. (1997). Paleostress reconstructions and geodynamics of the Baikal region, Central Asia, Part 2. Cenozoic rifting. *Tectonophysics*, 282(1-4): 1-38. [https://doi.org/10.1016/S0040-1951\(97\)00210-2](https://doi.org/10.1016/S0040-1951(97)00210-2).
- Diabat, A. A. (2007). Paleostress analysis of the Cretaceous-Tertiary rocks in central Jordan. *Dirasat, Pure Sciences*, 34(2):192-200.
- Diabat, A., and Masri, A. (2005). Orientation of the principal stresses along the Zerqa-Ma'in Fault. *Mu'tah Lil-Buhuth wad-Dirasat*, 20(1): 57-71.
- Fossen, H. (2016). *Structural geology*. 2nd Ed., Cambridge Univ. Press, Cambridge.
- Garfunkel, Z. (1981). Internal structure of the Dead Sea leaky transform (rift) in relation to plate kinematics. *Tectonophysics*, 80(1-4): 81-108. [https://doi.org/10.1016/0040-1951\(81\)90143-8](https://doi.org/10.1016/0040-1951(81)90143-8).
- Garfunkel, Z., Zak, I. and Freund, R. (1981). Active faulting in the Dead Sea rift. *Tectonophysics*, 80(1-4):1-26. [https://doi.org/10.1016/0040-1951\(81\)90139-6](https://doi.org/10.1016/0040-1951(81)90139-6).
- Hardy, C., Homberg, C., Eyal, Y., Barrier, É., and Müller, C. (2010). Tectonic evolution of the southern Levant margin since

- Mesozoic. *Tectonophysics*, 494(3 – 4):211–225. <https://doi.org/10.1016/j.tecto.2010.09.007>.
- Igwe, O., and Okonkwo, I. A. (2016). Application of paleostress analysis for the identification of potential instability precursors within the Benue Trough Nigeria. *Geoenvironmental Disasters*, 3(1): 1-15. <https://doi.org/10.1186/s40677-016-0051-z>
- Khalil, B. (1992). The geology of Ar Rabba area, scale 1: 50,000, sheet no. 3152– I. Natural Resources Authority, Amman, Jordan.
- Klinger, Y., Avouac, J. P., Dorbath, L., Karaki, N. A., and Tisnerat, N. (2000). Seismic behaviour of the Dead Sea fault along Araba valley, Jordan. *Geophysical Journal International*, 142(3): 769–782. <https://doi.org/10.1046/j.1365-246x.2000.00166.x>.
- Kohn, B., Weissbrod, T., Chung, L., Farley, K., and Bodorkos, S. (2019). Low-temperature thermochronology of francolite: Insights into timing of Dead Sea Transform motion. *Terra Nova*, 31(3): 205–219. <https://doi.org/10.1111/ter.12387>.
- Masri, I. A. (1997). The tectonic evolution of Ed Dhira Monocline-east of the Dead Sea. In *Terra Nostra. Proceeding's 13th GIF Meeting on The Dead Sea rift as a Unique Global Site*. Dead Sea, Israel.
- Masson, F., Hamiel, Y., Agnon, A., Klinger, Y., and Deprez, A. (2015). Variable behavior of the Dead Sea Fault along the southern Arava segment from GPS measurements. *Comptes Rendus Geoscience*, 347(4):161–169. <https://doi.org/10.1016/j.crte.2014.11.001>.
- Powell, J. H. (1988). The geology of the Karak area, scale 1: 50,000, sheet no. 3152– III. Natural Resources Authority, Amman, Jordan.
- Radaideh, O. M., and Melichar, R. (2015). Tectonic paleostress fields in the southwestern part of Jordan: New insights from the fault slip data in the southeastern flank of the Dead Sea Fault Zone. *Tectonics*, 34(9):1863–1891. <https://doi.org/10.1002/2015TC003919>.
- Simón, J. L. (2019). Forty years of paleostress analysis: has it attained maturity? *Journal of Structural Geology*, 125: 124–133. <https://doi.org/10.1016/j.jsg.2018.02.011>.
- Wallace, R. E. (1951). The geometry of shearing stress and relation to faulting. *The Journal of Geology*, 59(2): 118– 130. <https://doi.org/10.1086/625831>.
- Weinstein, Y., Nuriel, P., Inbar, M., Jicha, B. R., and Weinberger, R. (2020). The impact of the Dead Sea transforms kinematics on adjacent volcanic activity. *Tectonics*, 39(1): e2019TC005645. <https://doi.org/10.1029/2019TC005645>.
- Yamaji, A. (2007). *An Introduction to Tectonophysics: Theoretical Aspects of Structural Geology*. Terrapub, Tokyo.
- Zoback, M. L. (1992). First-and second-order patterns of stress in the lithosphere: The World Stress Map Project. *Journal of Geophysical Research: Solid Earth*, 97(B8): 11703–11728. <https://doi.org/10.1029/92JB00132>.